Journal of Porphyrins and Phthalocyanines
J. Porphyrins Phthalocyanines 2001; **5**: 323–333

NMR, IR, Mössbauer and quantum chemical investigations of metalloporphyrins and metalloproteins

LORI K. SANDERS, WILLIAM D. ARNOLD and ERIC OLDFIELD

[1]*Department of Chemistry, University of Illinois at Urbana-Champaign, 600 South Mathews Avenue, Urbana, IL 61801, USA*

Received 15 October 1999; Revised 10 March 2000
Accepted 15 March 2000

ABSTRACT: We review contributions made towards the elucidation of CO and O_2 binding geometries in respiratory proteins. Nuclear magnetic resonance, infrared spectroscopy, Mössbauer spectroscopy, X-ray crystallography and quantum chemistry have all been used to investigate the Fe–ligand interactions. Early experimental results showed linear correlations between ^{17}O chemical shifts and the infrared stretching frequency (ν_{CO}) of the CO ligand in carbonmonoxyheme proteins and between the ^{17}O chemical shift and the ^{13}CO shift. These correlations led to early theoretical investigations of the vibrational frequency of carbon monoxide and of the ^{13}C and ^{17}O NMR chemical shifts in the presence of uniform and non-uniform electric fields. Early success in modeling these spectroscopic observables then led to the use of computational methods, in conjunction with experiment, to evaluate ligand-binding geometries in heme proteins. Density functional theory results are described which predict ^{57}Fe chemical shifts and Mössbauer electric field gradient tensors, ^{17}O NMR isotropic chemical shifts, chemical shift tensors and nuclear quadrupole coupling constants (e^2qQ/h) as well as ^{13}C isotropic chemical shifts and chemical shift tensors in organometallic clusters, heme model metalloporphyrins and in metalloproteins. A principal result is that CO in most heme proteins has an essentially linear and untilted geometry ($\tau = 4°$, $\beta = 7°$) which is in extremely good agreement with a recently published X-ray synchrotron structure. CO/O_2 discrimination is thus attributable to polar interactions with the distal histidine residue, rather than major Fe–C–O geometric distortions. Copyright © 2001 John Wiley & Sons, Ltd.

KEYWORDS: hemoglobin; myoglobin; NMR; IR; Mössbauer; X-ray; density functional theory (DFT); metalloporphyrins; metalloproteins

INTRODUCTION

The nature of small ligand binding to metal centers in respiratory proteins has been investigated for several decades [1–10]. Small ligands with physiological function, such as O_2, CO, and NO, have been of particular interest. CO and NO act as regulators of cell and organ function [11] while O_2 is required for respiration and there has been particular interest in the discrimination in CO/O_2 binding by hemoglobin and myoglobin. CO binds much less strongly to metalloproteins than it does to metalloporphyrins, a fortunate circumstance since CO is produced *in vivo* as a product of porphyrin catabolism. A range of mechanisms has been postulated for this discrimination, including protein-induced distortion of the Fe–C–O bond [12] and hydrogen-bonding stabilization of bound O_2 by the distal ligand [6, 13, 14]. In addition, the metalloporphyrin distortions which have been reported in some heme proteins [15] can also be expected to influence ligand binding. However, the precise nature of these stabilizing/destabilizing effects has been difficult to evaluate at a molecular level, since the reliability of the protein structures is part of the debate [16]. There is, therefore, interest in employing both crystallographic [13–15] and spectroscopic methods to study structure and bonding in metalloproteins, using well-characterized model systems to help establish the structure–spectroscopic correlations. Spectroscopic methods such as infrared (IR) and Raman spectroscopy [16–18], nuclear magnetic resonance (NMR) [19–21], and Mössbauer spectroscopy [22–25] have each been used to provide basic structural information. In addition to these experimental techniques, quantum chemical methods have also been applied to related questions of molecular structure and function [26–40].

This article will review work done in this laboratory over the last 15 years which provides insight into the nature of small ligand binding to respiratory proteins. In particular, we have been interested in clarifying the structure of CO bound to heme proteins and how CO and O_2 are discriminated against in their binding. Spectroscopic observables including the ^{57}Fe NMR chemical shift, the ^{57}Fe Mössbauer quadrupole splitting, the ^{17}O NMR chemical shift, the ^{17}O nuclear quadrupole coupling, the ^{13}C NMR chemical shift, the ^{13}C NMR chemical shift anisotropy and the ^{13}C chemical shift tensor elements have all been obtained for model compounds, as well as in many cases for metalloproteins. These spectroscopic results and their theoretical interpretations will be reviewed.

*Correspondence to: E. Oldfield, Department of Chemistry, University of Illinois at Urbana-Champaign, 600 South Mathews Avenue, Urbana, IL 61801, USA.

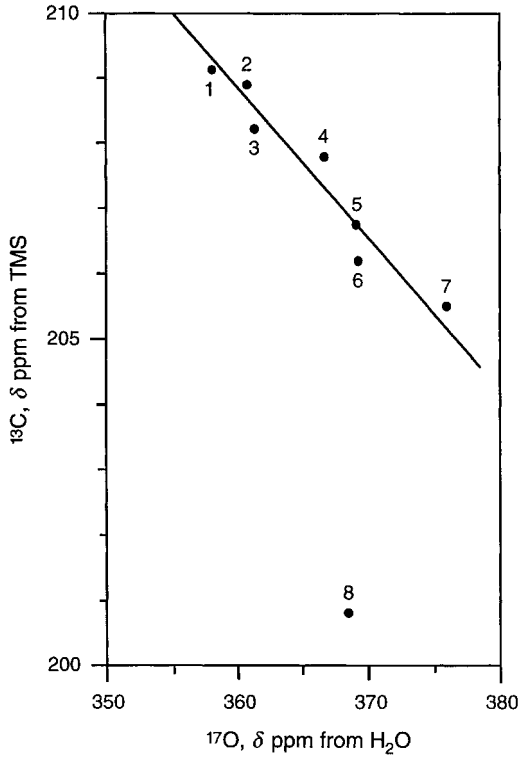

Fig. 1. Plot of ^{17}O NMR chemical shifts versus ^{13}C NMR chemical shifts of CO ligands in various hemoproteins. **(1)** CO-horseradish peroxidase isozyme C, pH = 6.4 [43]. **(2)** CO-horseradish peroxidase isozyme A, pH = 6.8 [43]. **(3)** Rabbit Hb α chain [42, 44]. **(4)** Sperm whale Mb [42, 44]. **(5)** Human Hb α chain [42, 44]. **(6)** Human Hb β chain and rabbit Hb β chain [42, 44]. **(7)** CO–picket fence porphyrin [42]. **(8)** CO–chloroperoxidase, pH = 5.8 [43]. (Reproduced by permission of The American Society for Biochemistry and Molecular Biology, Inc. from Lee HC, *et al. J. Biol. Chem.* 1988; **263**: 16 118.).

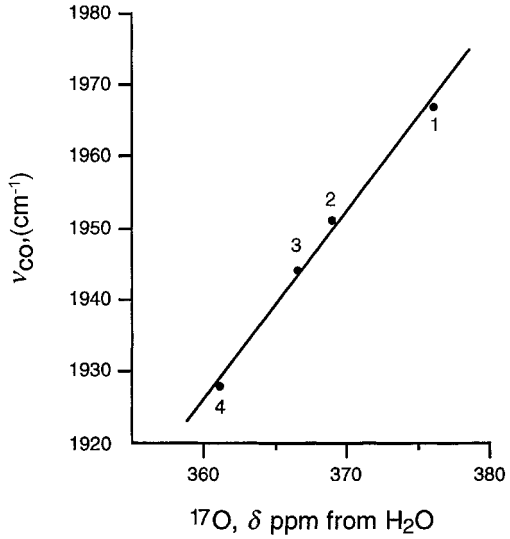

Fig. 2. Plot of the ^{17}O NMR chemical shifts versus infrared $^{12}C^{16}O$ stretching frequencies: **(1)** CO–picket fence porphyrin; **(2)** human α and β chains and rabbit Hb β chain; **(3)** sperm whale MbCO; **(4)** rabbit Hb α chain. (Reproduced with permission from Lee HC, Oldfield E. *J. Am. Chem. Soc.* 1989; **111**: 1584. Copyright 1989, The American Chemical Society.).

EARLY EXPERIMENTAL AND THEORETICAL RESULTS

Our earliest investigations of metal–ligand interactions in hemoproteins utilized ^{17}O NMR to probe the heme center of $C^{17}O$ ferrous peroxidases: horseradish peroxidase isozyme A, horseradish peroxidase isozyme C and chloroperoxidase [41]. Like hemoglobin and myoglobin, horseradish peroxidase systems contain iron–protoporphyrin IX, and can bind to a variety of ligands, both in the ferric and ferrous states. Chloroperoxidase is a heme protein which has spectral properties similar to cytochrome P-450 and has unique catalytic activities. An inverse linear correlation was seen between the ^{17}O chemical shifts of the heme-bound CO ligands and the corresponding ^{13}C chemical shifts, for a variety of heme proteins, including myoglobin, hemoglobin and horseradish peroxidases, as shown in Fig. 1 [42–44]. The one exception seen was in the behavior of CO–chloroperoxidase where the chemical shifts deviate markedly from the correlation, suggesting that structural differences may exist in the proximal side of the heme plane.

The first high-resolution ^{17}O NMR spectra of CO ligands bound to metalloproteins were observed in aqueous *Physeter catadon* ferrous myoglobin (sperm whale MbCO), adult human ferrous hemoglobin (HbCOA), and in *Oryctolagus cuniculus* ferrous hemoglobin (rabbit HbCO) [42]. Early structural analyses suggested that the Fe–CO unit in MbCO and HbCO is bent and/or tilted with respect to the porphyrin ring [12, 45, 46] whereas in heme model compounds the Fe–CO unit is linear and normal to the porphyrin plane [47]. Thus, it was proposed that steric hindrance due to amino acids on the distal side of the heme pocket resulted in a distortion of the Fe–CO geometry [48]. Due to the close proximity of the CO moiety to the distal residues in hemoproteins, ^{17}O NMR was expected to be an informative probe of these local structural effects on ligand binding affinities of hemoproteins in solution [42]. The NMR results showed an excellent linear correlation between the infrared CO stretching frequencies and ^{17}O NMR chemical shifts for bound CO in hemoproteins, as well as in the model compound CO–picket fence porphyrin (Fig. 2) [42]. This indicated that in the picket fence porphyrin, which is unhindered by protein side-chains, irreversible CO binding corresponded to a highly downfield shifted ^{17}O resonance and a higher frequency IR stretch, while the relatively unstable rabbit Hb α chain displayed the most upfield shifted NMR signal and a lower frequency IR stretch for CO. These differences were attributed to the degree of distal amino acid interaction with the heme-bound CO [42].

For nuclei with non-spherical charge distributions ($I \geq 1$), there may be an observable interaction between the nuclear quadrupole moment and the electric field gradient at the nucleus, termed nuclear quadrupole coupling, which may be manifested in nuclear spin relaxation rates. This early work resulted in the first experimental demonstration of multiexponential relaxation of a spin $I = 5/2$ nucleus and its analysis with relaxation theory in a system that was not complicated by the effects of chemical exchange [42]. The detailed analysis of the relaxation data led to a determination of the ^{17}O nuclear quadrupole coupling constant

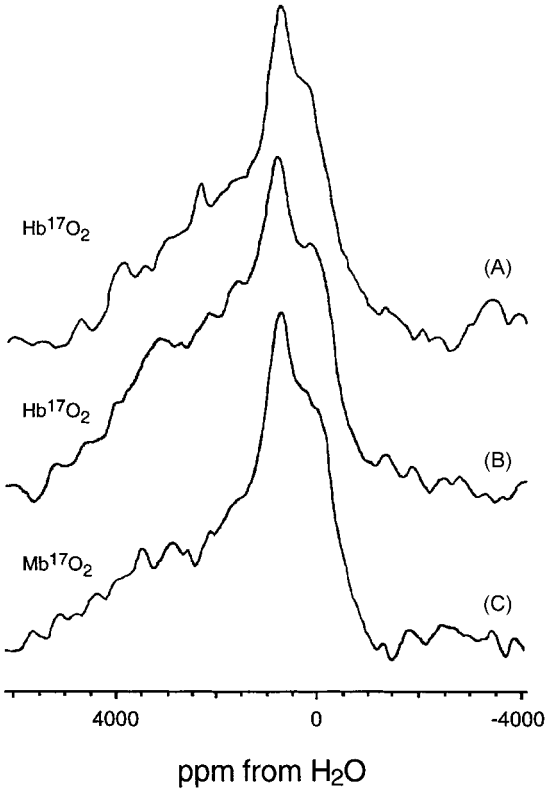

Fig. 3. 8.45 T ^{17}O NMR spectra at 77 K of [$^{17}O_2$]hemoglobin and myoglobin: **(A)** hemoglobin, frozen solution; **(B)** hemoglobin, polyethylene glycol microcrystals; **(C)** myoglobin, polyethylene glycol microcrystals. (Reproduced with permission from Oldfield E, *et al. J. Am. Chem. Soc*. 1991; **113**:8680. Copyright 1991, The American Chemical Society.).

(e^2qQ/h) of 0.95 MHz and a rotational correlation time (τ_c) of 14 ns for MbC^{17}O which indicated a rigid heme–CO unit in sperm whale carbonmonoxymyoglobin. For HbC^{17}O, the ^{17}O results gave $e^2qQ/h = 0.9$ MHz and $\tau_c = 23$ ns ($\omega_o\tau_c = 10$).

'Picket fence porphyrin' (5,10,15,20-tetrakis(α,α,α,α-*O*-pivalamidophenyl)(porphyrinato)Fe(II)), a model compound for the respiratory metalloproteins oxyhemoglobin and oxymyoglobin, was the subject of another early ^{17}O NMR investigation [19], which also included the first observation of ^{17}O NMR resonances of oxyhemoglobin and oxymyoglobin, shown in Fig. 3. The experimental lineshapes are dominated by the principal components of the ^{17}O chemical shift tensor, which in the case of oxypicket fence porphyrin revealed both highly shifted resonances and extremely large chemical shift anisotropies for both the bridging and nonbridging oxygens. While the low signal-to-noise ratios for the oxymyoglobin and oxyhemoglobin spectra did not warrant detailed spectral simulations, the spectra (Fig. 3) did show pronounced similarities with those of the picket fence porphyrin. The overall observed spectral breadths of ~4000 ppm, as well as the position of the major singularity, were both close to the values found for oxypicket fence porphyrin at low temperatures. These studies also demonstrated fast axial diffusion of the O_2 ligand at room temperature in the porphyrin system, from which an Fe–O–O bond angle of 140° could be deduced.

Iron-57 NMR has also been used as a probe of heme protein structure both in metalloproteins [49–51] and in model systems, by detection of the isotropic chemical shift (δ_i) as well as the chemical shift anisotropy ($|\delta_\perp - \delta_\parallel|$). In early work, Baltzer [50] studied the ^{57}Fe isotropic chemical shift in ^{57}Fe-labeled ferrocytochrome *c*, finding $\delta_i = 11\,197$ ppm, considerably deshielded from the $\delta_i = 8227$ ppm found in MbCO and Baltzer suggested that the chemical shift tensor element in the porphyrin plane ($\delta_\perp$) was ≈9000 ppm for MbCO, ferrocytochrome *c* and other high symmetry porphyrins. Baltzer also reasoned that it is primarily $\delta_\parallel$, the chemical shift tensor element perpendicular to the heme plane, which dominates the changes in δ_i with axial ligation. This specifically implied a change in sign of the anisotropy ($\delta_\perp - \delta_\parallel$) in going from MbCO to ferrocytochrome *c*. Additionally implied was the idea that heme proteins should exist that have $\delta_\perp \approx \delta_\parallel$, which would result in extremely long spin-lattice relaxation times (T_1). Chung *et al.* demonstrated that a series of alkyl isocyanide derivatives (ethyl isocyanide, isopropyl isocyanide and *n*-butyl isocyanide) of ferrous myoglobin indeed possess a T_1 an order of magnitude longer than previously seen in MbCO [51]. These results supported Baltzer's suggestion that there is a sign reversal of ^{57}Fe chemical shift anisotropy when moving from MbCO to ferrocytochrome *c*. The long T_1 values are due to a very small chemical shift anisotropy ($\delta_\perp \approx \delta_\parallel$) and these results can be attributed to MbCO containing a strongly π-bonding CO ligand, while ferrocytochrome *c* contains a much weaker π-bonding axial methionine ligand. Thus, chemical shift anisotropy, in addition to the isotropic chemical shift can be utilized to probe bonding interactions at the heme center, although the results of quantum calculations do not support the originally proposed tensor assignments, as noted below.

The examination of ligand–heme interactions in proteins then continued with a series of ^{17}O and ^{13}C NMR investigations of C^{17}O and ^{13}CO-labeled heme proteins [52]. Strong correlations between $\delta_i(^{17}O)$ and the IR stretching frequency, ν_{CO}, between the ^{17}O e^2qQ/h and ν_{CO} (Fig. 4) and between the ^{17}O e^2qQ/h and $\delta_i(^{17}O)$ (Fig. 5) were observed in a large number of CO–heme proteins. The linear relationships found between the ^{17}O e^2qQ/h and ν(C–O) or between the ^{17}O e^2qQ/h and $\delta_i(^{17}O)$ in heme proteins were not, however, typical of metal carbonyls, as reported in several other studies of CO bound to metallocarbonyls [53–56], with the metalloprotein results being much more correlated than those found in other systems. Although the correlations of $\delta_i(C^{17}O)$ with ν(C–O) were better than the correlations of $\delta(^{13}CO)$ with ν(C–O), it was shown that the four observables were all in fact interrelated and the argument was made that ^{13}C chemical shifts were dominated by changes in metal–carbon π-bonding, while the ^{17}O e^2qQ/h and $\delta_i(^{17}O)$ were a result of electrical polarization of CO by the (distal histidine's) charge field in the protein. These results also implied that the changes seen in chemical shift and vibrational frequency from one system to another were not the result of a wide range of ligand tilts and bends reported in some crystallographic studies, [12, 45, 48]. These results therefore formed the basis for more detailed studies, including the origins of the frequency shifts seen experimentally.

THEORETICAL INVESTIGATIONS OF ν(C–O)–δ_i CORRELATIONS

The NMR–IR correlations were then investigated theoretically via *ab initio* calculations using Hartree–Fock theory,

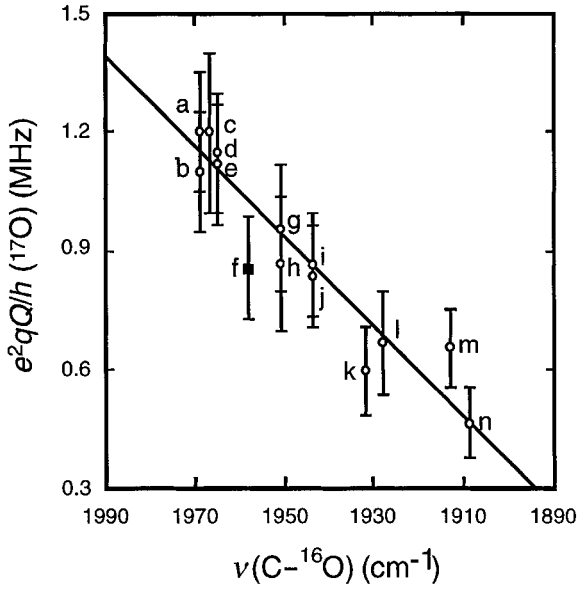

Fig. 4. Graph showing relation between ν(C–O) and ^{17}O e^2qQ/h for CO-liganded heme proteins. **(a)** Synthetic *P. catadon* myoglobin, His E7 → Val; **(b)** synthetic *P. catadon* myoglobin, His E → Val; **(c)** picket fence porphyrin; **(d)** synthetic *P. catadon* myoglobin, His E7 → Phe; **(e)** synthetic *P. catadon* myoglobin, His E7 → Phe; **(f)** chloroperoxidase, pH = 6; **(g)** human *P. catadon* myoglobin; **(h)** rabbit hemoglobin, β chain; **(i)** *P. catadon* myoglobin; **(j)** *P. catadon* myoglobin; **(k)** horseradish peroxidase isoenzyme A, pH = 9.5; **(l)** rabbit hemoglobin, α chain; **(m)** horseradish peroxidase isoenzyme C, pH = 7.0; **(n)** horseradish peroxidase isoenzyme A, pH = 4.5. Multiple entries for some proteins reflect scatter in individual T_1 determinations. (Reproduced with permission from Park KD, *et al. Biochemistry* 1991; **30**:2333. Copyright 1991, The American Chemical Society.).

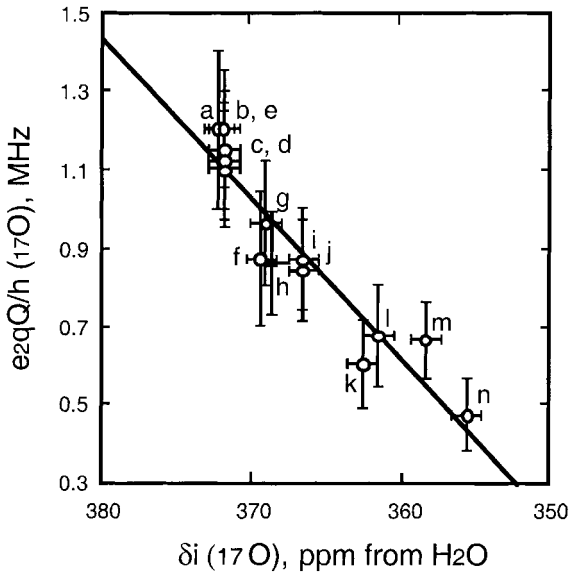

Fig. 5. Graph showing relation between $\delta_i(^{17}O)$ and $e^2qQ/h(^{17}O)$ for C^{17}O-labelled heme proteins. **(a)** Picket fence porphyrin; **(b)** synthetic *P. catadon* myoglobin, His E7 → Val; **(c)** synthetic *P. catadon* myoglobin, His E7 → Phe; **(d)** synthetic *P. catadon* myoglobin, His E7 → Phe; **(e)** synthetic *P. catadon* myoglobin, His E7 → Val; **(f)** rabbit hemoglobin, β chain; **(g)** human adult hemoglobin; **(h)** chloroperoxidase, pH = 6; **(i)** *P. catadon* myoglobin; **(j)** *P. catadon* myoglobin; **(k)** horseradish peroxidase isoenzyme A, pH = 9.5; **(l)** rabbit hemoglobin α chain; **(m)** horseradish isoenzyme C, pH = 7.0; **(n)** horseradish peroxidase isoenzyme A, pH 4.5. Multiple entries for some proteins reflect scatter in individual T_1 determinations. (Reprinted with permission from Park KD. *et al. Biochemistry* 1991; **30**:2333. Copyright 1991, The American Chemical Society.).

resulting in a proposed model of the distal ligand effects found in carbonmonoxy heme proteins [57, 58]. The vibrational transition frequencies and the chemical shielding tensors were robustly determined as functions of several types of external potentials: a uniform electric field, an electric field gradient and a field associated with an electric dipole oriented either parallel or perpendicular to the CO axis. The changes in ν(C–O) as a result of the applied electrical perturbations were attributed to the changes in the equilibrium bond length induced by the electric fields. The NMR chemical shifts were also affected by the applied electrical perturbations. Interestingly, in the presence of a uniform field, the ^{13}C and ^{17}O chemical shifts moved in opposite directions with the applied field. However, in the presence of an applied field gradient, the ^{13}C and ^{17}O chemical shifts changed in the same direction. These effects are the result of different types of electrical polarization. An applied electric field along the molecular axis induces a dipole that shifts charge along the axis. Thus, charge density increases at one end of the molecule, resulting in increased shielding, and decreases at the other end of the molecule, resulting in decreased chemical shielding. Conversely, a field gradient induces a quadrupole moment, which influences the charge density at both nuclei of the CO moiety similarly. This investigation also revealed a linear correlation between the vibrationally averaged ^{17}O nuclear quadrupole coupling constant $<e^2qQ/h>$ and the vibrational frequency, due to electrical polarization.

The correlations seen between ν_{CO} and the NMR observables $\delta_i(^{17}O)$, $\delta_i(^{13}C)$ and e^2qQ/h were in agreement with the correlations seen experimentally in heme–CO [52] and supported the electrical polarization model of distal ligand effects in heme proteins. This theoretical model was later supported by a density functional theory (DFT) investigation of $\delta_i(^{17}O)$, $\delta_i(^{13}C)$ and ν(C–O) of CO bound to Fe^{2+} in the presence of an electric field [59].

DFT INVESTIGATION OF METAL ION NMR AND ^{57}Fe MÖSSBAUER QUADRUPOLE SPLITTINGS

Early theoretical investigations from this laboratory led to the idea of utilizing quantum chemical methods to calculate chemical shifts of amino acid residues in proteins [60], as well as investigating chemical shifts of nuclei associated with the metal centers of metalloporphyrins and metalloproteins. It was shown that it is possible to calculate chemical shifts of individual amino acid residues of proteins without a detailed knowledge of the complete protein structure, and that this is a consequence of the chemical shielding being a rather local or short-range property [60]. It was therefore thought that predicting chemical shifts via quantum chemistry, or more precisely relating predicted chemical shifts to structure, could result in new approaches to protein structure determination in general, as well as in

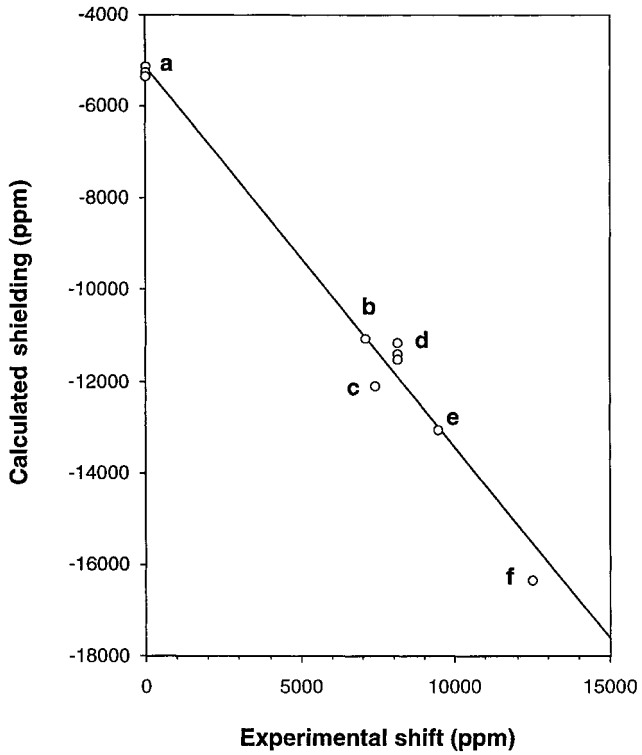

Fig. 6. Graph showing correlation between experimental ^{59}Co NMR chemical shifts and theoretical shieldings. Slope = −0.83 and $R^2 = 0.98$. **(a)** $[Co(CN)_6]^{3-}$; **(b)** $[Co(en)_3]^{3+}$; **(c)** $[Co(NO_2)_6]^{3-}$; **(d)** $[Co(NH_3)_6]^{3+}$; **(e)** $[Co(NH_3)_4CO_3]^{+}$; and **(f)** $Co(acac)_3$. (Reprinted with permission from Godbout N, Oldfield E. *J. Am. Chem. Soc.* 1997; **119**:8065. Copyright 1997, The American Chemical Society.).

predicting more accurate metal–ligand binding geometries in heme proteins, in particular.

In order to accurately predict chemical shifts and electric field gradients of the heme center of hemoproteins, a methodology needed to be developed and validated for computing the spectroscopic properties of metal atoms in proteins and model systems, since the early quantum chemical investigations were only performed on the lighter elements ^{1}H, ^{13}C, ^{15}N, ^{17}O, and ^{19}F. First, it was found to be necessary to switch from Hartree–Fock *ab initio* methods to density functional theory (DFT) methods, which effectively include electron correlation and electron exchange in the calculations at reasonable computational cost. It was then necessary to determine the most accurate and cost effective combination of basis sets and exchange-correlation functionals required for the calculation of the chemical shielding and electric field gradient tensors of the metal centers and attached ligands.

Density functional theory (DFT) methods were first used to predict the isotropic ^{59}Co NMR chemical shifts in a series of Co(III) (d^6) complexes: $[Co(NO_2)_6]^{3-}$, $[Co(CN)_6]^{3-}$, $[Co(NH_3)_6]^{3+}$, $[Co(NH_3)_4CO_3]^{+}$, $Co(acac)_3$ (acac = acetylacetonate), and $[Co(en)_3]^{3+}$ (en = ethylenediamine) [61]. The structures chosen were those which appeared to be well refined, and purely experimental geometries were used for the calculations. Becke's three parameter functional [62] with the Lee, Yang, and Parr correlation functional [63] (B3LYP hybrid exchange correlation functional) was used together with a Wachters' basis set [64] for cobalt atoms, and a 6-31G* basis set [65] was used for all other atoms. For the isotropic ^{59}Co NMR chemical shifts, the average reported solution NMR experimental shifts were used [66]. The ^{59}Co chemical shifts were well reproduced by the calculations as shown in Fig. 6 (slope = −0.83, $R^2 = 0.98$). In addition to the isotropic chemical shifts, it was also possible to accurately predict the principal elements of the ^{59}Co shielding tensors (σ_{11}, σ_{22}, σ_{33}), the absolute shieldings of $Co(CN)_6^{3-}$ and $Co(acac)_3$, and the Co–C bond length shielding derivative for $Co(CN)_6^{3-}$. These results for a d^6 transition metal were most encouraging in that the ability to successfully predict chemical shift trends, absolute shieldings and shielding tensor elements for Co(III) transition metal complexes opened up new possibilities for probing the spectroscopic properties of other metal ions in biological systems by combined use of NMR spectroscopy and quantum chemistry.

This ^{59}Co NMR study was followed by a theoretical investigation of the ^{57}Fe NMR spectra and ^{57}Fe Mössbauer quadrupole splittings in two metalloporphyrins containing (bis)pyridine and (bis)trimethylphosphine ligands, as well as in a series of model compounds of cytochrome *c*, isopropyl isocyanide myoglobin, and carbonmonoxymyoglobin [67]. A locally dense basis set scheme [68] was used to evaluate the ^{57}Fe chemical shieldings and electric field gradients at the iron center. The Wachters' all electron representation was used for iron [64], a 6-311++G(2d) basis for all atoms directly attached to the iron center, a 6-31G* basis for the second shell peripheral atoms, and a 3-21G basis for the remaining peripheral atoms [65]. These basis sets were used in conjunction with the B3LYP hybrid exchange-correlation functional [62, 63] for all calculations. The theoretical results were compared to experimental chemical shifts and Mössbauer quadrupole splittings. Good agreement was found between theory and experiment for the cytochrome *c* and myoglobin ^{57}Fe NMR chemical shifts and shift tensors, which encouraged us to perform an additional series of calculations in order to test the sensitivity of these chemical shieldings to structure, exchange-correlation functional and basis set variations [67]. The largest effect was seen due to variations in the exchange-correlation functional. Changes in local geometry, such as a change in C–O bond length, had a more modest effect on the results of the calculations. The ^{57}Fe chemical shift tensor orientations were generally close to molecular symmetry axes, although reversed from previous work, but with the skew of the shielding tensor again reversing sign on transition from strong to weak ligand fields. Also, the results showed that the paramagnetic contribution overwhelmingly dominated the total absolute shielding, as noted in previous work [70]. Interestingly, when MbCO models having distorted Fe–C–O geometries (as seen in protein X-ray crystal structures) were employed, the experimental ^{57}Fe chemical shifts were in poor accord with the theoretical results. This suggested that the Fe–C–O bond is close to the porphyrin normal, and was not as distorted as is seen in many protein crystal structures. As discussed below, we then extended these calculations to enable us to deduce the ligand tilt and bend angles with some accuracy.

The detailed theoretical investigation of ^{57}Fe NMR chemical shifts was accompanied by a theoretical examination of the ^{57}Fe Mössbauer quadrupole splitting, ΔE_Q [67]. Could we accurately predict Mössbauer splittings in metalloporphyrins and metalloproteins using similar computational methodology to that used in the chemical shift

calculations? The Mössbauer quadrupolar splitting is related to the components of the electric field gradient tensor (EFG) as follows:

$$\Delta E_{\mathrm{Q}} = \frac{1}{2} eQV_{zz}\left(1 + \frac{\eta^2}{3}\right)^{1/2}$$

where e is the electron charge, Q the quadrupole moment of the $I^* = 3/2$ excited state and the principal components of the EFG at Fe are defined such that V_{zz} is the largest component of the EFG tensor. By convention:

$$|V_{zz}| \geq |V_{yy}| \geq |V_{xx}|$$
$$\text{and } V_{xx} + V_{yy} + V_{zz} = 0$$

and η is the asymmetry parameter of the electric field gradient:

$$\eta = \frac{V_{xx} - V_{yy}}{V_{zz}}$$

The DFT calculation yielded a 1.31 mm s^{-1} ^{57}Fe Mössbauer splitting for ferrocytochrome *c*, which is in very good agreement with the experimental value of 1.2 mm s^{-1} [69]. The calculations also reproduced the very small splitting values for the RNC and CO adducts of myoglobin seen experimentally [67]. These results not only supported the use of DFT methods for the analysis of Mössbauer quadrupole splitting data, but also encouraged the continued exploration of metalloporphyrin and metalloprotein structural questions using a combined DFT, NMR and Mössbauer spectroscopic approach.

The ^{57}Fe quadrupole splittings in a series of 14 organometallic and heme-model compounds were next investigated, including $Fe(CO)_3$(*cyclo*-butadiene), $Fe(CO)_3$(propenal), $Fe(CO)_5$, Fe(TPP)(CO)(1-MeIm), $Fe(TPP)(py)_2$, Fe(TPP)(CO)(py), Fe(TPP)(PhNO)(py), and $Fe(OEP)(PMe_3)_2$, where TPP = 5,10,15,20-tetraphenylporphinato, 1-MeIm = 1-methylimidizole, py = pyridine, PhNO = nitrosobenzene, OEP = 2,3,7,8,12,13,17,18-octaethylporphinato and PMe_3 = trimethyl-phosphine [71]. Once again, the electric field gradient tensor at the iron nucleus was evaluated by using a locally dense basis approach [68] with a Wachters' all electron basis [64] on iron, a 6-311 ++ G(2d) basis on all atoms directly bonded to the iron and a 6-31G* basis for all other atoms in the organometallic compounds. For the metalloporphyrins, a 6-31G* basis was used for the first shell atoms and a 3-21G* basis on all other atoms. The EFGs were calculated using the B3LYP hybrid exchange correlation functional [62, 63].

Using a value of 0.16×10^{-28} m^2 for the quadrupole moment of ^{57}Fe, we found excellent agreement between theoretical and experimental Mössbauer quadrupole splittings, with a slope of 1.04, an R^2 value of 0.975, and an RMSD of 0.18 mm s^{-1} for the 14 compounds evaluated. These results provided additional support for the use of quantum chemical methods in the investigation of Mössbauer quadrupole splittings.

It was also noted that the calculated quadrupole splitting of the heme-model compound, Fe(TPP)(CO)(1-MeIm) (0.35 mm s^{-1}), was extremely close to the 0.36–0.37 mm s^{-1} observed in carbonmonoxymyoglobin and carbonmonoxyhemoglobin [25]. Since the model compound has a linear and untilted Fe–C–O angle [71], this similarity supported the idea of a linear and untilted Fe–C–O bond in heme proteins, contrary to most crystallographic structures and textbook pictures. In order to test the hypothesis that the Fe–C–O is in fact linear and untilted, we investigated $\Delta E_{\mathrm{Q}}(^{57}\mathrm{Fe})$ as a function of Fe–C–O ligand tilt and bend in Fe(TPP)(CO)(1-MeIm). For each of five tilt/bend structures, the Fe–C and C–O bond lengths were geometry optimized. The results of these optimizations indicated that the C–O bond lengths are constant over a 40° range of tilt/bend geometries, while the Fe–C bond lengths are not. The $\Delta E_{\mathrm{Q}}(^{57}\mathrm{Fe})$ was found to be close to experiment at two conformations: 0° tilt/0° bend and 20° tilt/20° bend. However, the energy for the 20° tilt/20° bend structure was 11 kcal higher than in the linear structure, implying linear and untilted geometries in proteins. The calculations were also able to accurately predict the orientations of the principal components of the ^{57}Fe electric field gradient tensor, and in the case of MbCO, the largest component (V_{zz}) was found to be oriented perpendicular to the porphyrin plane, as found experimentally [72].

Having established that DFT accurately predicts the NMR chemical shifts and quadrupole splittings at metal centers, we subsequently investigated the use of DFT methods in describing ^{13}C and ^{17}O NMR shieldings and ^{17}O nuclear quadrupole coupling constants in four metal–CO compounds containing terminal and bridging CO ligands: $Fe(CO)_5$, $Fe_2(CO)_9$, $Ni_2(\eta^5\text{-}C_5H_5)_2(CO)_2$ and $Rh_6(CO)_{16}$ [73]. The nuclear shieldings were calculated by using the sum-over-states density functional perturbation theory (SOS-DFPT) approach in the LOC1 approximation [28–31] with individual gauges for localized orbitals (IGLO) [74] using the deMon program [75]. Experimental values were obtained from solid state NMR spectra, which represented the first such measurement of the principal elements of the ^{13}C and ^{17}O shielding tensors in $Fe(CO)_5$, and of the ^{17}O e^2qQ/h in all four compounds. The resulting correlations between DFT calculations and experimental NMR data were all very strong. For ^{13}C, we found a slope of 0.98 and an R^2 value of 0.92 for δ_{iso}, and a slope of 0.99 and an R^2 value of 1.00 for δ_{ii}. For ^{17}O, we found a slope of 0.89 and an R^2 value of 0.94 for δ_{iso}, a slope of 0.96 and an R^2 value of 1.00 for δ_{ij}, and a slope of 1.1 and an R^2 value of 0.96 for the ^{17}O e^2qQ/h. The calculations also generated information regarding the orientation of the shift tensors with respect to the molecular framework. An unexpected result was seen in the orientation of the oxygen chemical shift tensors of the bridging carbonyl ligands in $Fe_2(CO)_9$. The most deshielded chemical shift component was found to be along the C–O axis which is highly unusual for a carbonyl ligand.

The ^{13}C and ^{17}O shieldings and ^{17}O quadrupole coupling constants were next evaluated in several iron(II), ruthenium(II), and osmium(II) carbonyl derivatives of 5,10,15,20-tetraphenylporphyrinate (TPP) [76]. Each of the following compounds was synthesized and then characterized via single-crystal X-ray diffraction: Fe(TPP)(CO)(1-MeIm), Ru(TPP)(CO)(1-MeIm), Os(TPP)(CO)(1-MeIm), and Os(TPP)(CO)(Py), where (1-MeIm) = 1-methylimidazole, and py = pyridine. The structures of the three (TPP)(1-MeIm) compounds displayed major saddle distortions, with the extent of deviation from planarity being Fe > Ru ≅ Os, but the planarity of the porphyrin ring in the pyridine complex was about an order of magnitude less than for the 1-MeIm complexes. Using DFT, together with the experimental X-ray atomic coordinates, we calculated the ^{13}C and ^{17}O chemical shielding and ^{17}O e^2qQ/h for the CO moiety in each of these compounds, and compared the results to the experimental solid state NMR measurements. The correla-

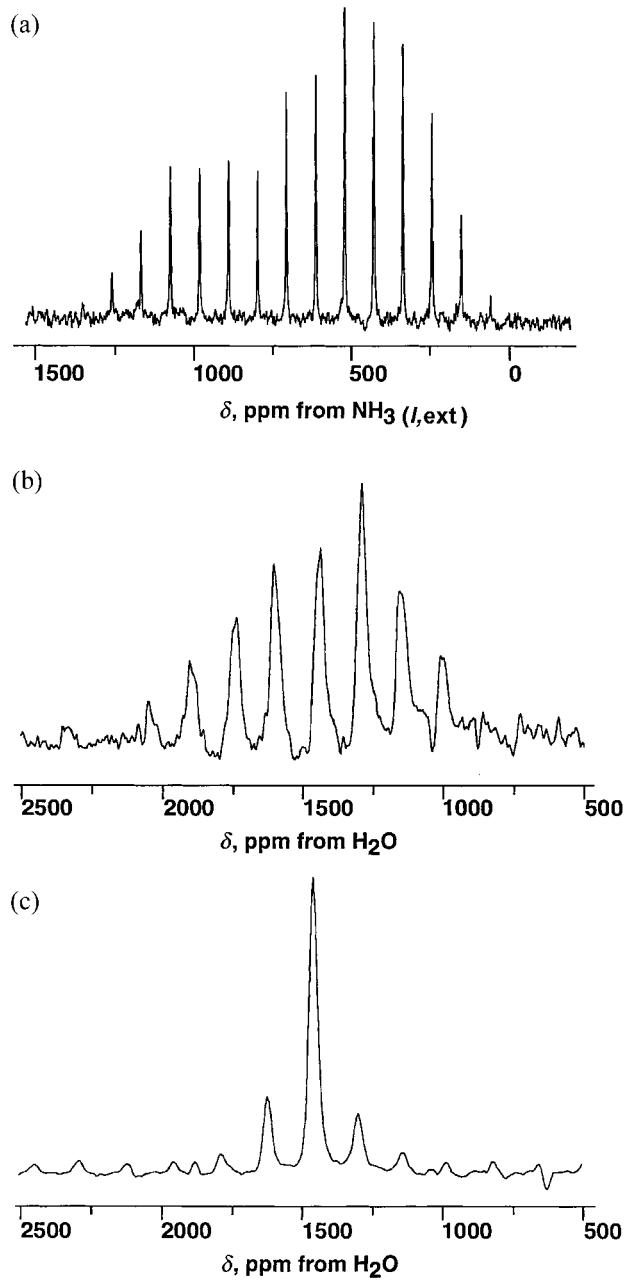

Fig. 7. Representative NMR spectra of metalloporphyrins investigated. **(a)** 8.45 T ^{15}N MAS NMR spectrum of Fe(TPP)(Ph^{15}NO)(py) at 298 K. **(b)** 11.7 T ^{17}O MAS NMR spectrum of Co(OEP)(N^{17}O) at 373 K. **(c)** 11.7 T ^{17}O MAS NMR spectrum of Co(TPP)(N^{17}O) at 298 K. (Reproduced with permission from Godbout N. *et al. J. Am. Chem. Soc*. 1999; **121**:3829. Copyright 1999, The American Chemical Society.).

tions between theory and experiment were excellent, with both $\delta_{iso}(^{13}C)$ and $\delta_{iso}(^{17}O)$ yielding correlation coefficients of *ca* 0.99, although the slopes were somewhat less than ideal (^{13}C, slope = −0.97; ^{17}O, slope = −1.27). For the ^{17}O quadrupole coupling constant, e^2qQ/h, our results revealed only a 0.20 MHz RMS deviation between theory and experiment [76].

In order to probe the origins of heme ruffling in proteins, we synthesized an additional series of metalloporphyrins: Fe(OEP)(CO)(1-MeIm), Ru(OEP)(CO)(1-MeIm), Os(OEP)(CO)(1-MeIm), and Fe(TPP)(iPrNC)(1-MeIm), where OEP = 2,3,7,8,12,13,17,18-octaethylporphyrinate [77]. We then characterized these compounds with X-ray diffraction, solid-state NMR, and DFT. Unlike the (TPP)(CO)(1-MeIm) systems [76] these four complexes were found to have basically planar porphyrin rings. These results suggested the following rule for these and closely related systems [77]: 'that in order for there to be a porphyrin distortion there needs to be one and only one repulsive interaction between a porphyrin ring substituent and an axial ligand.' We can also express this rule as a formula in terms of logic operations:

$$f(\mathrm{A,B,C}) = \mathrm{A} \cdot \mathrm{B} \oplus \mathrm{C}$$

Here A represents a porphyrin ring substitution (e.g. phenyl in TPP), and B and C are the axial substituents of the metal center. The logical AND operation is represented by the ·symbol, while the logical exclusive OR operation is represented by the ⊕ symbol. By assigning to each axial and equatorial substituent (A, B, and C) a one or a zero, we found that this formula predicts whether or not a metalloporphyrin's porphyrin ring will be distorted from planarity. The assignment of substituents is as follows:

1: PhNO, NODMA, CCl_2, 1-MeIm, phenyl (equatorial ring);
0: CO, NO, pyridine, ethyl (equatorial ring)

For example, if A = 1, B = 0, and C = 1, as is the case for Fe(TPP)(CO)(1-MeIm), then $f(\mathrm{A,B,C}) = 1 \cdot 0 \oplus 1 = 1$ and porphyrin ring ruffling is predicted. If, however, A = 1, B = 0, C = 0, as is the case for Fe(TPP)(CO)(py), then $f(\mathrm{A,B,C}) = 1 \cdot 0 \oplus 0 = 0$ (no ruffling predicted). This logical rule allowed the successful prediction of porphyrin ring ruffling in each of the 16 metalloporphyrins examined [77].

We also gathered solid-state magic angle spinning (MAS) NMR data for a variety of metalloporphyrins including Fe(OEP)(CO)(1-MeIm), Ru(OEP)(CO)(1-MeIm), Os(OEP)(CO)(1-MeIm), and Fe(TPP)(iPrNC)(1-MeIm) with appropriately enriched ligands: ^{13}CO, C^{17}O, iPrN^{13}C, and iPr^{15}NC. These data were then compared with DFT predictions of ^{13}C, ^{15}N, and ^{17}O δ_{iso}, and δ_{ii}, and we found the following correlations: slope = 1.18, $R^2 = 0.99$ for $\delta_{ii}(^{13}C)$; slope = 1.01, $R^2 = 1.00$ for $\delta_{ii}(^{15}N)$; slope = 1.32, $R^2 = 0.99$ for $\delta_{iso}(^{17}O)$ [77].

These correlations, established by using well-characterized FeCO (and FeCO analog) porphyrin models of metalloproteins, address one aspect of the issue of preferential O_2/CO binding in metalloproteins and as noted above, our results support linear, untilted binding in CO heme proteins. In order to investigate the binding of O_2 in such systems, we synthesized several Fe–O_2 analog metalloporphyrins: Fe(TPP)(PhNO)(1-MeIm), Fe(TPP)(PhNO)(py), Fe(TPP)(NODMA)(py), Fe(OEP)(PhNO)(1-MeIm), and Co(OEP)(NO), where NODMA = 4-nitroso-*N, N*-dimethylaniline [78]. We used single-crystal X-ray diffraction to obtain accurate structural information on each compound, and noted that the f(A,B,C) rule correctly predicted the presence or absence of ruffling in the porphyrin ring. We then acquired solid-state MAS NMR (representative spectra are shown in Fig. 7) data on these compounds, labeled with Ph^{15}NO, ^{15}NO–NODMA, ^{15}NO, and N^{17}O, and compared the resulting shifts with those obtained by using DFT together with the crystallographically determined atomic coordinates (with H substituted for Ph). In this way, we tested our ability to compute the NMR spectroscopic observables in Fe–O_2 analog metalloporphyrins. The NMR and DFT computed shielding tensors were

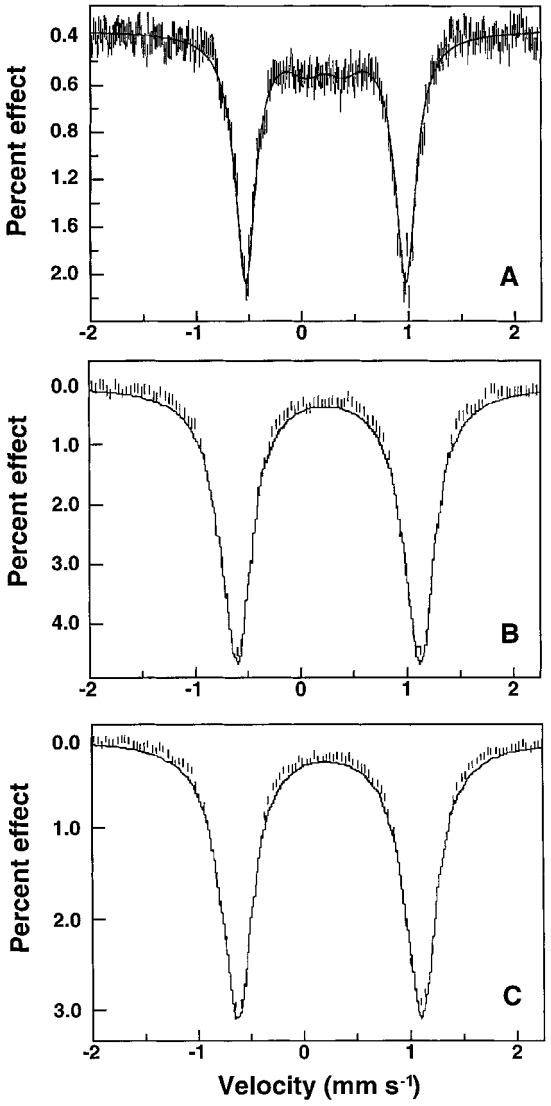

Fig. 8. Representative ^{57}Fe Mössbauer spectra. **(a)** Fe(TPP)(NODMA)(py), at 298 K; **(b)** [^{57}Fe] Mb·PhNO at 50 K; **(c)** [^{57}Fe] Mb·PhNO at 200 K. (Reproduced with permission from Godbout N. *et al. J. Am. Chem. Soc*. 1999; **121**:3829. Copyright 1999, The American Chemical Society.).

again highly correlated. For the δ_{ii} of the R^{15}NO structures we found a slope of 0.91 and an R^2 value of 0.99; for Co^{15}NO, a slope of 1.09 and an R^2 value of 1.00; and for CoN^{17}O, a slope of 1.23 and an R^2 value of 0.99 for the theory-versus-experiment correlations, which gives some confidence in the quality of the DFT calculations in these systems.

The porphyrin Fe center was also exploited as a probe of O_2 ligand binding, via DFT and Mössbauer spectroscopic determinations of the ^{57}Fe ΔE_Q. Using the X-ray crystal structures of these Fe–O_2 analogs, we found that DFT computed quadrupole splittings ranged between -0.98 and -1.4 mm s^{-1}, while the corresponding experimental Mössbauer quadrupole splittings had a range between -1.3 and -1.5 mm s^{-1} as seen in the representative spectra shown in Fig. 8. The RMS deviation between the theoretical and experimental ΔE_Q was only $\sim$0.2 mm s^{-1} consistent with our previous results [71]. This success with the isoelectronic Fe–O_2 analogs, Fe(RNO)/Fe(HNO), prompted our application of DFT methods to directly investigate the Fe–O_2 containing oxypicket fence porphyrin and oxymyoglobin. Such a study was more problematic, however, since the atomic coordinates of both systems were much less reliable than those of our measured analog complexes. As with most protein crystal structures, the structure of oxymyoglobin (MbO_2) has considerable uncertainty relative to small molecule structures, while the crystal structure of oxypicket fence porphyrin (O_2·PFP) suffers from a high degree of disorder [79]. In addition, the measured Mössbauer ΔE_Q(^{57}Fe) in both O_2·PFP and MbO_2 is temperature dependent, which was not the case for Mb·PhNO (Fig. 8) [78]. The room temperature ΔE_Q of O_2·PFP is about $|1.3|$ mm s^{-1}, while the 4 K value is -2.1 mm s^{-1} [22]. Similarly, MbO_2 has splittings of $|1.6|$ mm s^{-1} at 260 K but -2.3 mm s^{-1} at 4 K [25]. Several models have been proposed for this ΔE_Q temperature dependence, including harmonic bond oscillations [25, 80], rotational diffusion [81], and a site jump between different substates [22]. Specifically, it has been suggested that O_2·PFP exists in two substates, one being characterized as having a ΔE_Q of ~-2 mm s^{-1}, the other having a ΔE_Q of $\sim$0.9 mm s^{-1} [22].

Given the lack of crystallographically well-characterized atomic coordinates as DFT input, we performed a multitude of calculations to assess the sensitivity of the computed properties to a variety of structural and computational variables. We investigated both planar and nonplanar porphyrin rings, optimized and nonoptimized geometries, several 1-MeIm/O_2 torsions with respect to the porphyrin ring, and several basis sets and functionals. This relatively comprehensive set of calculations ($N = 18$) produced an average ΔE_Q of -2.2 ± 0.4 mm s^{-1}, which is in good agreement with the *ca* 4 K Mössbauer data. With the knowledge that the O_2 moiety undergoes fast axial rotation in O_2·PFP, as revealed by NMR [23], we were then able to predict, via DFT, a motionally averaged ΔE_Q of 1.21 mm s^{-1}, which is very close to the room temperature O_2·PFP ΔE_Q of $|1.3|$ mm s^{-1} [78].

One long-debated explanation for the preferential binding of O_2 over CO has been that, once bound, O_2 is stabilized by hydrogen bonding to a distal ligand in the metalloprotein [82]. Simple, atom-based charges, such as Mulliken populations, are commonly employed in molecular modeling. However, in reality a molecular charge distribution gives rise to a complex, three-dimensional electrostatic potential, $\Phi(r)$, and it is thus desirable to test such a stabilization model over a full $\Phi(r)$ surface. It has been established that quantum chemical molecular electrostatic potentials are excellent representations of those derived experimentally, from high-angle, high-resolution X-ray diffraction [83, 84]. We therefore used DFT to calculate $\Phi(r)$ and the charge density, $\rho(\mathbf{r})$, in model Fe–CO, Fe–O_2, and Fe–PhNO metalloporphyrins [78]. Plate 1 compares these potentials, mapped onto iso-surfaces of $\rho(\mathbf{r})$. The results show a clear difference in $\Phi(\boldsymbol{r})$ between Fe–CO and Fe–O_2; the more negative potential (darker blue) being found with O_2. A -0.09 a.u. electrostatic potential is exhibited at the terminal O-atom in the O_2 ligand, while at CO the potential is -0.06 a.u. These results strongly suggest that bound O_2 provides a better hydrogen bond acceptor than bound CO, and thus may be more effectively stabilized via interaction with a distal metalloprotein ligand (e.g. the distal histidine in myoglobin and hemoglobin).

Another hypothesis for CO/O_2 binding discrimination in metalloproteins is that the steric hindrance from a distal histidine residue compels CO to bind to the iron center in a

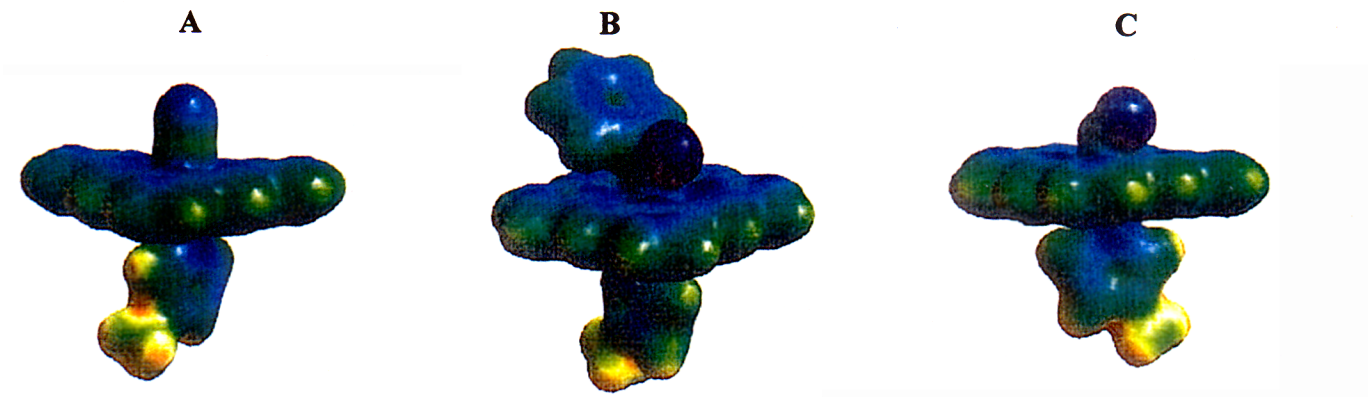

Plate 1. Electrostatic potential surfaces, $\Phi(r)$, mapped onto a 0.017 a.u. charge density surface, $\rho(r)$, for: (**A**) Fe(P)(CO)(1-MeIm); (**B**) Fe(P)(PhNO)(1-MeIm); and (**C**) Fe(P)(O_2)(1-MeIm). The dark-blue color in the case of O_2 and PhNO indicates a large negative electrostatic potential. The electrostatic potential on CO is –0.06 a.u. on the carbonyl oxygen in **A** but –0.086 a.u. in the oxy complex **C**, and –0.10 a.u. in the PhNO adduct, **B**. The electrostatic potential surfaces are plotted for values between –0.06 and 0.17 a.u. (Reproduced with permission from Godbout N. *et al. J. Am. Chem. Soc.* 1999; **121**: 3829. Copyright 1999, The American Chemical Society.)

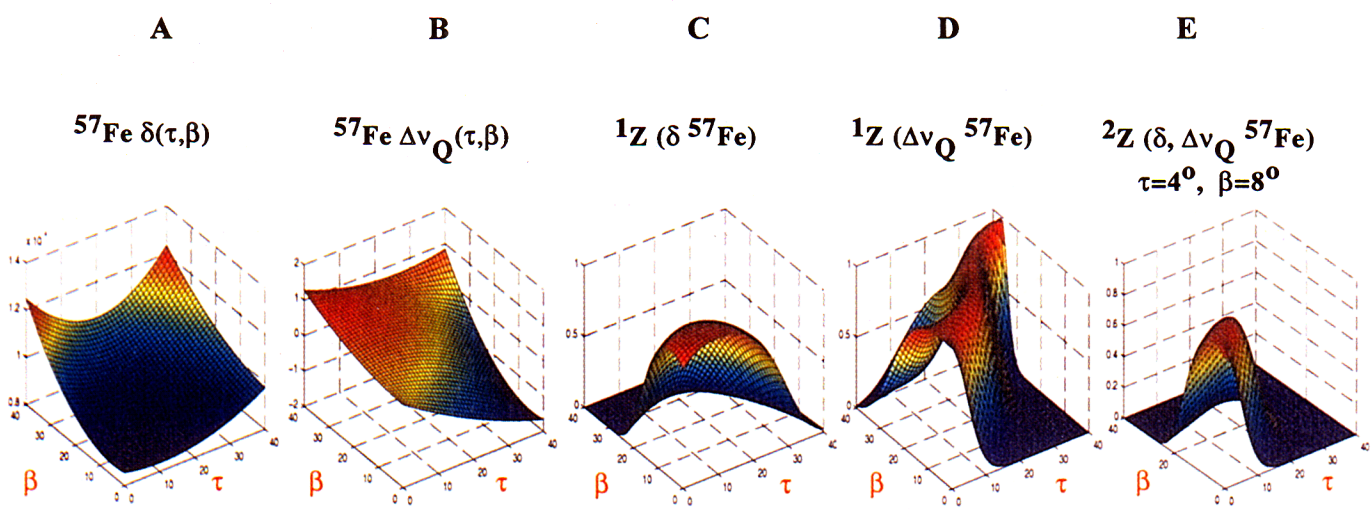

Plate 2. Property and probability surfaces for A_1 protein conformational substate. (**A**) ^{57}Fe NMR chemical shift. (**B**) ^{57}Fe Mössbauer quadrupole splitting. (**C**) ^{57}Fe NMR chemical shift ^{1}Z probability surface. (**D**) ^{57}Fe Mössbauer quadrupole splitting ^{1}Z probability surface. (**E**) ^{2}Z probability surface (^{57}Fe NMR chemical shift, ^{57}Fe Mössbauer quadrupole splitting).

tilted and/or bent fashion, as does O_2 [6, 82]. In a free heme unit outside the protein, CO is bound to iron in a linear manner, making an Fe–C–O angle of $\sim 180°$ and an angle with the porphyrin plane of $\sim 90°$. The idea of a bent/tilted CO in metalloproteins has been used to explain the fact that CO binds about 25 000 times more strongly to model metalloporphyrins than does O_2, but only about 250 times more strongly in hemoglobin and myoglobin [6, 82, 85]. While there has been crystallographic, NMR, Mössbauer spectroscopic and other evidence in support of a distorted protein Fe–C–O [6, 86–96], there has also been crystallographic, NMR, IR, and Raman evidence to the contrary [16, 17, 52, 57, 58]. Our approach to this problem was to first investigate metalloporphyrin model compounds whose structures are very well characterized, and which have the same spectroscopic observables as metalloproteins. Quantum chemical calculations of these observables were then validated against experiment for these well-defined model compounds. Once their validity at discrete geometries could be established, the calculations were then expanded to consider the complete spatial/geometric dependence of a given spectroscopic observable. Thus, we can obtain a property surface for each spectroscopic parameter which represents that parameter as a function of, for example, the tilt, τ, and bend, β, of the Fe–C–O group. We then use a Bayesian probability approach [97] to convert each parameter surface into a Z-surface, which represents the probability that the parameter arises from a specific point in (τ,β) space. Furthermore, these single parameter Z-surfaces can be multiplied together to form a higher order, conditional probability surface, the maximum being the τ,β solution for a given set of spectroscopic observables. We had previously found success using this technique to predict the backbone torsion angles ϕ and ψ in tripeptides [98]. By measuring the alanine $^{13}C^{\alpha}$ chemical shift tensor in Gly–Ala–Val, we were able to predict, via calculated Z-surfaces, a backbone geometry for Gly–Ala–Val which fell within 12° of the crystallographically determined geometry [98]. This prediction was made on the basis of only one solid-state NMR measurement, and it seems reasonable to suppose that including much more spectroscopic information would increase the accuracy of the method.

With the idea of predicting the Fe–C–O geometry in metalloproteins, we therefore began an examination of seven relevant spectroscopic observables [99]: $\delta_i(^{13}C)$, the isotropic ^{13}C NMR chemical shift; $\Delta\delta(^{13}C)$, the ^{13}C NMR shift anisotropy; $\delta_i(^{17}O)$, the isotropic ^{17}O NMR chemical shift; $e^2qQ/h(^{17}O)$, the ^{17}O nuclear quadrupole coupling constant; $\delta_i(^{57}Fe)$, the isotropic ^{57}Fe NMR chemical shift; $\Delta E_Q(^{57}Fe)$, the ^{57}Fe Mössbauer quadrupole splitting; and ν_{CO}, the Fe–C–O IR stretching frequency. Our investigation focused on trying to predict the tilt and bend angles of Fe–C–O in the two most studied substates of heme proteins: A_0 and A_1. We first measured the ^{13}C and ^{17}O NMR spectroscopic observables in the linear Fe–C–O system Fe(TPP)(CO)(1-MeIm), where 1-MeIm = 1-methylimidazole, and found that they were very similar to those of the A_0 substate of carbonmonoxymyoglobin (MbCO). The $\delta_i(^{13}C)$ of the CO ligand in Fe(TPP)(CO)(1-MeIm) was 205 ppm, and $|\delta_{33}-\delta_{11}|$ was 453 ppm, to be compared with the $\delta_i(^{13}C)$ of 205.5 ppm and the $|\sigma_{33}-\sigma_{11}|$ of 435 ppm seen in MbCO (A_0) [99]. The $\delta_i(^{17}O)$ and $e^2qQ/h(^{17}O)$ determined from a variety of A_0 heme proteins [52] were 372 ± 1 ppm and 1.1 MHz, respectively, compared to the 372 ppm and 1.0 MHz found in the TPP adducts. In addition to these NMR parameters, both the stretching frequency ν_{CO} and the Mössbauer $\Delta E_Q(^{57}Fe)$ in Fe(TPP)(CO)(1-MeIm) agree with the corresponding A_0 heme protein values [52].

While this agreement between observables seen in the *linear* FeCO TPP and those in the A_0 heme proteins implied that FeCO is indeed linear in A_0 proteins, it was still theoretically possible that other τ,β values could give rise to the same observables. In order to determine if the observables predicted a unique linear τ,β solution, we applied the Bayesian probability approach [97]. NMR parameters were calculated as functions of tilt and bend by using DFT on a model Fe(bis(amidinato))(CO)(1-MeIm) system, and the resulting parameter surfaces were converted into Z-surface probabilities. We took the product of four of these ^1Z surfaces and formed a ^4Z probability surface:

$$^4Z(\tau,\beta) = {}^1Z(^{13}C,\delta_i)\,{}^1Z(^{13}C,|\delta_{33}-\delta_{11}|)\,{}^1Z(^{17}O,e^2qQ/h)$$

which predicted a single τ,β region ($\tau = \beta \leq 2°$) from which all four spectroscopic observables could simultaneously arise [99] in the A_0 substate. A simple demonstration of the Z-surface approach for just two parameters is shown in Plate 2.

We therefore concluded that Fe–C–O is linear in the A_0 substate of MbCO and other heme proteins. For the A_1 substate, however, the situation was more complex because we lacked an A_1 model metalloprotein. Fortunately, additional experimental data (Mössbauer quadrupole splitting, $\Delta E_Q(^{57}Fe)$, and the ^{57}Fe isotropic chemical shift, $\delta_i(^{57}Fe)$) were available for the A_1 substate [25, 49, 100]. In addition, there are known ^{13}C and ^{17}O NMR chemical shift, ^{17}O NMR quadrupolar coupling constant, and ν_{CO} stretch frequency differences between the A_0 and A_1 substates [99]. By including uniform field and point charge perturbations in our calculations, we were able to show that these spectroscopic differences were primarily due to electric field effects. Consequently, using the same Bayesian probability approach as for the A_0 substate, and including the ^{57}Fe information (Plate 2), we created a ^6Z solution for the A_1 substate:

$$^6Z(\tau,\beta) = {}^1Z(^{13}C,\delta_i)\,{}^1Z(^{13}C,|\delta_{33}-\delta_{11}|)\,{}^1Z(^{17}O,\delta_i)^1 \times Z(^{17}O,e^2qQ/h)\,{}^1Z(^{57}Fe,\delta_i)\,{}^1Z(^{57}Fe,\Delta E_Q)$$

The highest probability solution for ^6Z predicts a linear and untilted Fe–C–O: $\tau = 4°$, $\beta = 7°$ [99]. This predicted geometry was confirmed shortly afterwards by a synchrotron X-ray diffraction study on sperm whale MbCO, which found $\tau = 4.7\ (0.9)°$ and $\beta = 7.4\ (1.9)°$ [101].

CONCLUSION

The combined use of experimental and quantum chemical techniques has led to successful structure prediction not only in small systems [98] but also in ligand binding in heme proteins [99]. The determination of an essentially linear and untilted Fe–C–O bond angle in the MbCO A_1 substate and its validation by synchrotron crystallography [101] provides excellent support for the utilization of a combined theoretical/experimental approach in the investigation of heme protein structure–function relationships. While not yet exploited, in addition to providing static structural information, theoretical methods generate considerable electronic structure information, including molecular orbitals, charge densities $\rho(\mathbf{r})$, and laplacians of the

charge densities, $\nabla^2\rho(\mathbf{r})$ [78]. Recent work also suggests that this approach can be applied to paramagnetic systems [102], providing a probe of the electronic structures of respiratory proteins such as ferric cytochrome *c*, deoxyhemoglobin and deoxymyoglobin. The power of the experimental–theoretical approach promises to provide valuable new structural, bonding and electronic information in future metalloprotein investigations.

Acknowledgements

This work was supported by the United States Public Health Service (National Institutes of Health Grants HL-19481 and GM-50694), and by the National Center for Supercomputing Applications (funded in part by United States National Science Foundation Grant CHE-970020N).

REFERENCES

1. Pauling L, Coryell CD. *Proc. Natl. Acad. Sci. USA* 1936; **22**: 210.
2. Pauling L. *Nature* 1964; **203**: 182.
3. Weiss JJ. *Nature* 1964; **203**: 182.
4. Jameson GB, Molinaro FS, Ibers JA, Collman JP, Brauman JI, Rose E, Suslick KS. *J. Am. Chem. Soc.* 1978; **100**: 6769.
5. Collman JP, Gagne RR, Reed CA, Robinson WT, Rodley GA. *Proc. Natl. Acad. Sci.* 1974; **71**: 1326.
6. Springer BA, Sligar SG, Olson JS, Phillips GN Jr,. *Chem. Rev.* 1994; **94**: 699.
7. Sage JT. *J. Biol. Inorg. Chem.* 1997; **2**: 537.
8. Slebodnick C, Ibers JA. *J. Biol. Inorg. Chem.* 1997; **2**: 521.
9. Lim M, Jackson TA, Anfinrud PA. *J. Biol. Inorg. Chem.* 1997; **2**: 531.
10. Spiro TG, Kozlowski PM. *J. Biol. Inorg. Chem.* 1997; **2**: 516.
11. Suematsu M, Wakabayashi Y. *Cardiovas. Res.* 1996; **32**: 679.
12. Kuriyan J, Wilz S, Karplus M, Petsko GA. *J. Mol. Biol.* 1986; **192**: 133.
13. Phillips SEV, Schoenborn BP. *Nature* 1981; **292**: 81.
14. Nagai K, Luisi B, Shih D, Miyazaki G, Imai K, Poyart C, DeYoung A, Kwiatkowsky L, Noble RW, Lin S-H, Yu N-T *Nature* 1987; **329**: 858.
15. Shaanan BJ. *J. Mol. Biol.* 1983; **171**: 31.
16. Ray GB, Li X-Y, Ibers JA, Sessler JL, Spiro TG. *J. Am. Chem. Soc.* 1994; **116**: 162.
17. Lim M, Jackson TA, Anfinrud PA. *Science* 1995; **269**: 962.
18. Hirota S, Li T, Phillips GN, Olson JS, Mukai M, Kitagawa TJ. *J. Am. Chem. Soc.* 1996; **118**: 7845.
19. Oldfield E, Lee HC, Coretsopoulos C, Adebodun F, Park KD, Yang S, Chung J, Phillips B. *J. Am. Chem. Soc.* 1991; **113**: 8680.
20. Gerothanassis IP, Barrie PJ, Momenteau M, Hawkes GE. *J. Am. Chem. Soc.* 1994; **116**: 11944.
21. Barrie PJ, Gerothanassis IP, Momenteau M, Hawkes GE. *J. Magn. Reson.* 1995; **108**: 185.
22. Spartalian K, Lang G, Collman JP, Gagne RR, Reed CA. *J. Chem. Phys.* 1975; **63**: 5375.
23. Kirchner RF, Loew GH. *J. Am. Chem. Soc.* 1977; **99**: 4639.
24. Maeda Y, Harami T, Morita Y, Trautwein A, Gonser U. *J. Chem. Phys.* 1981; **75**: 36.
25. Debrunner PG. In *Iron Porphyrins*, Lever ABP, Gray HB. (eds). VCH: New York, 1989; 139.
26. Pulay P, Hinton JF, Wolinski K. *Nuclear Magnetic Shieldings and Molecular Structure*, Tossell JA. ed., Kluwer: Netherlands, 1993; 243.
27. Frisch MJ, Trucks GW, Schlegel HB, Gill PMW, Johnson BG, Robb MA, Cheeseman JR, Keith T, Petersson GA, Montgomery JA, Raghavachari K, Al-Laham MA, Zakrzewski VG, Ortiz JV, Foresman JB, Cioslowski J, Stefanov BB, Nanyakkara A, Challacombe M, Peng CY, Ayala PY, Chen W, Wong MW, Andres JL, Replogle ES, Gomperts R, Martin RL, Fox DJ, Binkley JS, Defrees DJ, Baker J, Stewart JP, Head-Gordon M, Gonzalez C, Pople JA. GAUSSIAN 94, Revision E.2, Gaussian, Inc.: Pittsburgh, PA, 1997.
28. Malkin VG, Malkina OL, Salahub DR. *Chem. Phys. Lett.* 1993; **204**: 87.
29. Malkin VG, Malkina OL, Casida ME, Salahub DR. *J. Am. Chem. Soc.* 1994; **116**: 5898.
30. Kaupp M, Malkin VG, Malkina OL, Salahub DR. *J. Am. Chem. Soc.* 1995; **117**: 1851.
31. Kaupp M, Malkin VG, Malkina OL, Salahub DR. *J. Am. Chem. Soc.* 1995; **117**: 8492.
32. Bühl, M. *Chem. Phys. Lett.* 1997; **267**: 251.
33. Schreckenbach G, Ziegler T. *J. Phys. Chem.* 1995; **99**: 606.
34. Rovira C, Ballone P, Parrinello M. *Chem. Phys. Lett.* 1997; **271**: 247.
35. Rovira C, Kunc K, Hutter J, Ballone P, Parrinello M. *J. Phys. Chem.* 1997; **101**: 8914.
36. Ghosh A, Bocian DF. *J. Phys. Chem.* 1996; **100**: 6363.
37. Vangberg T, Bocian DF, Ghosh A. *J. Biol. Inorg. Chem.* 1997; **2**: 526.
38. Jewsbury P, Yamamoto S, Minato T, Saito M, Kitagawa T. *J. Phys. Chem.* 1995; **99**: 12677.
39. Strohmeier M, Orendt AM, Facelli JC, Solum MS, Pugmire RJ, Parry RW, Grant DM. *J. Am. Chem. Soc.* 1997; **119**: 7114.
40. Vogel KM, Kozlowski PW, Zgierski MZ, Spiro TG. *J. Am. Chem. Soc.* 1999; **121**: 9915.
41. Lee HC, Cummings K, Hall K, Hager LP, Oldfield E. *J. Biol. Chem.* 1988; **263**: 16 118.
42. Lee HC, Oldfield E. *J. Am. Chem. Soc.* 1989; **111**: 1584.
43. Behere DV, Gonzalez-Vergara E, Goff HM. *Biochem. Biophys. Res. Commun.* 1985; **131**: 607.
44. Moon RB, Richards JH. *Biochemistry* 1974; **13**: 3437.
45. Norvell JC, Nunes AC, Schoenborn BP. *Science* 1975; **190**: 568.
46. Bianconi A, Congiu-Castellano A, Durham PJ, Hasnain SS, Phillips S. *Nature* 1985; **318**: 685.
47. Peng SM, Ibers JA. *J. Am. Chem. Soc.* 1976; **98**: 8032.
48. Collman JP, Brauman JI, Halbert TR, Suslick KS. *Proc. Natl. Acad. Sci. USA* 1976; **73**: 3333.
49. Lee HC, Gard JK, Brown TL, Oldfield E. *J. Am. Chem. Soc.* 1985; **107**: 4087.
50. Baltzer L, Becker ED, Tschudin RG, Gansow OA. *J. Chem. Soc. Chem. Commun.* 1985; **15**: 1040.
51. Chung J, Lee HC, Oldfield E. *J. Magn. Res.* 1990; **90**: 149.
52. Park KD, Guo K, Adebodun F, Chiu ML, Sligar SG, Oldfield E. *Biochemistry* 1991; **30**: 2333.
53. Aime S, Gobetto R, Osella D, Milone L, Hawkes GE, Randall EW. *J. Chem. Soc. Chem. Commun.* 1983; **13**: 794.

54. Aime S, Gobetto R, Osella D, Milone L, Hawkes GE, Randall EW. *J. Chem. Soc. Dalton Trans.* 1984; **9**: 1863.
55. Hawkes GE, Lian LY, Randall EW, Sales KD, Aime S. *J. Chem. Soc. Dalton Trans.* 1985; **1**: 225.
56. Aime S, Botta M, Gobetto R, Osella D. *J. Chem. Soc. Dalton Trans.* 1988; **3**: 791.
57. Augspurger JD, Dykstra CE, Oldfield E. *J. Am. Chem. Soc.* 1991; **113**: 2447.
58. Oldfield E, Guo K, Augspurger JD, Dykstra CE. *J. Am. Chem. Soc.* 1991; **113**: 7537.
59. de Dios AC, Earle EM. *J. Phys. Chem.* 1997; **101**: 8132.
60. de Dios AC, Pearson JG, Oldfield E. *Science* 1993; **260**: 1491.
61. Godbout N, Oldfield E. *J. Am. Chem. Soc.* 1997; **119**: 8065.
62. Becke AD. *J. Chem. Phys.* 1993; **98**: 5648.
63. Lee C, Yang W, Parr RG. *Phys. Rev. B* 1988; **37**: 785.
64. Wachters AJH. *J. Chem. Phys.* 1970; **52**: 1033.
65. Hehre WJ, Radom L, Schleyer P, Pople JA. In *Ab Initio Molecular Orbital Theory*; Wiley: New York, 1986.
66. Harris RK, Mann BE. (eds) In *NMR and the Periodic Table*; Academic Press, London, UK 1978.
67. Godbout N, Havlin R, Salzmann R, Debrunner PG, Oldfield E. *J. Phys. Chem. A* 1998; **102**: 2342.
68. Chesnut DB, Moore KD. *J. Comput. Chem.* 1989; **10**: 648.
69. Cooke R, Debrunner P. *J. Phys. Chem.* 1968; **48**: 4532.
70. Polam JR, Wright JL, Christensen KA, Walker FA, Flint H, Winkler H, Grodzicki M, Trautwein AX. *J. Am. Chem. Soc.* 1996; **118**: 5272.
71. Havlin RH, Godbout N, Salzmann R, Wojdelski M, Arnold W, Schulz CE, Oldfield E. *J. Am. Chem. Soc.* 1998; **120**: 3144.
72. Parak F, Thomanek UF, Bade D, Wintergerst B. *Z. Naturforsch. Ser. C* 1977; **32**: 501.
73. Salzmann R, Kaupp M, McMahon MT, Oldfield E. *J. Am. Chem. Soc.* 1998; **120**: 4771.
74. Kutzelnigg W, Fleischer U, Schindler M. *NMR-Basic Principles and Progress*, 1990; vol. **23**. Springer, Heidelberg.
75. Salahub DR, Duarte H, Godbout N, Guan J, Jamorski C, Leboeuf M, Malkin V, Malkina O, Sim F, Vela A. deMon Software, Université de Montréal, 1997.
76. Salzmann R, Ziegler CJ, Godbout N, McMahon M, Suslick KS, Oldfield E. *J. Am. Chem. Soc.* 1998; **120**: 11 323.
77. Salzmann R, McMahon MT, Godbout N, Sanders LK, Wojdelski M, Oldfield E. *J. Am. Chem. Soc.* 1999; **121**: 3818.
78. Godbout N, Sanders LK, Salzmann R, Havlin RH, Wojdelski M, Oldfield E. *J. Am. Chem. Soc.* 1999; **121**: 3829.
79. Jameson GB, Rodley GA, Robinson WT, Gagne RR, Reed CA, Collman JP. *Inorg. Chem.* 1978; **17**: 850.
80. Boso B, Debrunner PG, Wagner GC, Inubushi T. *Biochim. Biophys. Acta* 1984; **791**: 244.
81. Wise WW, Debrunner PG. *Bull. Am. Phys. Soc.* 1984; **29**: 365.
82. Stryer L. *Biochemistry*, Fourth Edition, 1995; Freeman WH. New York.
83. Flaig R, Koritsanszky T, Zobel D, Luger P. *J. Am. Chem. Soc.* 1998; **120**: 2227.
84. Koritsánszky T, Flaig R, Zobel D, Krane H-G, Morgenroth W, Luger P. *Science* 1998; **279**: 356.
85. Olson JS, Phillips GN Jr,. *J. Biol. Inorg. Chem.* 1997; **2**: 544.
86. Hanson JC, Schoenborn BP. *J. Mol. Biol.* 1981; **153**: 117.
87. Steigemann W, Weber E. *J. Mol. Biol.* 1979; **127**: 309.
88. Huber R, Epp O, Formanek H. *J. Mol. Biol.* 1970; **52**: 349.
89. Yang F, Phillips GN Jr,. *J. Mol. Biol.* 1996; **256**: 762.
90. Powers L, Sessler JL, Woolery GL, Chance B. *Biochemistry* 1984; **23**: 5519.
91. Durham P, Bianconi A, Castellano AC, Giovannelli A, Hasnain SS, Incoccia L, Morante S, Pendry JB. *EMBO J.* 1983; **2**: 1441.
92. Ascone I, Bianconi A, Dartyge E, Longa SD, Fontaine A, Momenteau M. *Biochim. Biophys. Acta* 1987; **915**: 168.
93. Lian T, Locke B, Kitagawa T, Nagai M, Hochstrasser RM. *Biochemistry* 1993; **32**: 5809.
94. Ormos P, Braunstein D, Frauenfelder H, Hong MK, Lin S-L, Sauke TB, Young RD. *Proc. Natl. Acad. Sci. USA* 1988; **85**: 8492.
95. Braunstein DP, Chu K, Egeberg KD, Frauenfelder H, Mourant JR, Nienhaus GU, Ormos P, Sligar SG, Springer BA, Young RD. *Biophys. J.* 1993; **65**: 2447.
96. Trautwein A, Maeda Y, Harris FE, Formanek H. *Theor. Chim. Acta* 1974; **36**: 67.
97. Le H, Pearson JG, deDios AC, Oldfield E. *J. Am. Chem. Soc.* 1995; **117**: 3800.
98. Heller J, Laws DD, Tomaselli M, King DS, Wemmer DE, Pines A, Havlin RH, Oldfield E. *J. Am. Chem. Soc.* 1997; **119**: 7827.
99. McMahon MH, deDios AC, Godbout N, Salzmann R, Laws DD, Le H, Havlin RH, Oldfield E. *J. Am. Chem. Soc.* 1998; **120**: 4784.
100. LaMar GN, Dellinger CM, Sankar SS. *Biochem. Biophys. Res. Commun.* 1985; **128**: 628.
101. Kachalova GS, Popov AN, Bartunik HD. *Science* 1999; **284**: 475.
102. Godbout N, Oldfield E. Unpublished results.